2014 IEEE International Conference on Robotics & Automation (ICRA)
Hong Kong Convention and Exhibition Center
May 31 - June 7, 2014. Hong Kong, China

Comparison of Ornithopter Wind Tunnel Force Measurements with Free Flight

Cameron Rose and Ronald S. Fearing

Abstract— **Developing models of flapping-winged fliers in free flight is vital for accurate control. The aerodynamics associated with flapping-winged flight are complex. Hence, a look-up table flight force model from wind tunnel data is a practical approach. In this work, we compare the flight of an ornithopter micro aerial vehicle (MAV), using free flight data collected from a Vicon motion capture system, to measured wind tunnel force and moment values. We compare the two data sets at equilibrium as a metric to determine the quality of the wind tunnel flight force estimation.**

To compare the two data sets, we find the predicted equilibrium angle of attack and velocity for the ornithopter in free flight. For a given flapping frequency and pitch control elevator deflection angle at free flight equilibrium, we compute the level sets at zero for pitch moment, net horizontal force, and net vertical force from the wind tunnel data. We then use the point on the zero moment level set that minimizes the vertical and horizontal force. The angle of attack and velocity at this minimal point are the wind tunnel predicted equilibrium point and are compared to the analogous free flight equilibrium point. We determined that the wind tunnel underestimates the angle of attack of the equilibrium point observed in free flight by 15 degrees, while the equilibrium velocity has an error of 0.1 m/s between the two sets at an average flight speed of 2 m/s.

I. INTRODUCTION

The aerodynamics of flapping-winged flight are nonlinear and complex, and are difficult to model. The flapping of the wings creates an unsteady airflow around the control surfaces of the flier, increasing the complexity of the aerodynamics associated with the surfaces [1][2][3][4]. An understanding of the behavior of these fliers in free flight is necessary for successful control.

One method of understanding the flight behavior of these fliers involves modeling the wing motion during each wing stroke, e.g. using blade element theory [5][6][7]. Another method involves multi-body modeling to account for the changing mass distribution as the flier flaps its wings [8][9][10].

We desire a simplified representation of the aerodynamics which can be used for on-board model-based control in 10 gram scale fliers. The previous control strategies used for ornithopters of this scale were based upon Proportional-Integral-Differential (PID) control schemes for target tracking or height regulation [11][12]. Information about the aerodynamic interactions of the ornithopter can produce a more robust model that can be used in more sophisticated control schemes such as Linear-Quadratic Regulator (LQR) or Model Predictive Control (MPC).

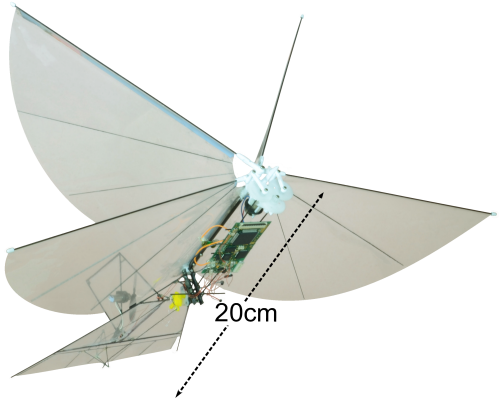

Fig. 1. The H^{2}Bird ornithopter [19].

For this aerodynamic modeling, it is necessary to collect data that can be used to estimate the behavior of the MAV over time. Common approaches to develop these models include averaging the flight behavior over the wing beat period, and using linear low-dimensional models to predict the flight behavior over time. It has been shown that using time averaged aerodynamic data is a valid approximation over a given wing stroke [13][14]. Wind tunnels are often used to measure aerodynamic properties of robotic fliers. Although some of the degrees of freedom are constrained by the mounting mechanism, this method of aerodynamic force and moment measurement has been used by previous researchers for the purpose of developing aerodynamic models for simulation and control. A simulation of insect flight for the Robofly project uses aerodynamic models based upon wind tunnel measurements [15][16]. In addition, mounted sensor measurements have also been used to measure the aerodynamic properties of wings for modelling by Khan and Agrawal [17]. Lee and Han recently implemented a non-contact magnetic suspension and balance system to control the attitude of an experimental model [18]. This setup allows for data collection and controller verification using selected degrees of freedom.

An alternative method to using stationary wind tunnel data for modeling is collecting free flight telemetry data using a motion tracking system. Humbert et al. utilized this method to create a dynamic model for their "Slow Hawk" ornithopter [20]. The flight data collected was used to fit parameters to a multi-body dynamic model, and wind tunnel

*This material is based upon work supported by the U.S. Army Research Laboratory under the Micro Autonomous Systems and Technology Collaborative Technology Alliance, and the National Science Foundation under Grant No. IIS-0931463

The authors are with the Department of Electrical Engineering and Computer Sciences, University of California, Berkeley, 94708, USA {c_rose,ronf}@eecs.berkeley.edu

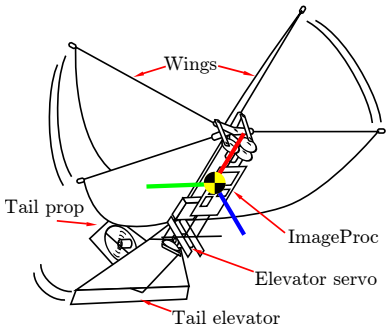

Fig. 2. H^{2}Bird ornithopter with attitude control axes and labeled control surfaces [19].

tests were used to determine the associated aerodynamic model. This method, however, involves the fitting of many model parameters.

In this paper, we consider both an experimental data set collected at equilibrium free-flight conditions and a wind tunnel data set for an ornithopter. We compare the flight conditions of the free-flight equilibrium and the wind tunnel predicted equilibrium to determine if the wind tunnel data can be utilized to accurately predict the free flight of the ornithopter in future simulation models.

II. ROBOTIC PLATFORM

A. H^{2}Bird Ornithopter

The robotic platform used is a flapping-winged MAV known as the H^{2}Bird (Fig. 1) [19]. The H^{2}Bird has a custom built carbon fiber frame, carbon fiber reinforced clap-fling wings, and carbon fiber reinforced tail, and uses the Silverlit i-Bird RC flier power train[1]. The wingspan of the H^{2}Bird is 26.5 cm and its mass is 13.6 grams. Yaw and pitch control are provided by a tail-mounted propeller and servo-controlled elevator, respectively (Fig. 2). For control and sensing, the H^{2}Bird uses an on-board ImageProc 2.4[2] controller that includes a 40 MIPS microprocessor, 6 DOF IMU, IEEE 802.15.4 radio, and motor drivers, powered by a 90 mAH lithium polymer battery [11].

B. Attitude Control

The attitude estimation and control of the H^{2}Bird are both performed on-board. This process is depicted in Fig. 3 in the internal control block, and is computed at 300Hz. To estimate the pose of the H^{2}Bird, the angular rate values measured by the on-board gyroscope are integrated over time. Separate proportional-integral-derivative (PID) controllers use the estimated pose and the desired pitch (θ) and yaw angles, provided by an external source, to determine the necessary control surface inputs to the elevator servo and tail propeller motor to achieve the desired pose. Another PID controller is used to regulate the flap frequency of the H^{2}Bird, with the desired frequency provided by the external source, and flap frequency estimated by a Hall effect sensor on an output gear of the transmission, as inputs.

[1]Silverlit Toys Manufactory Ltd.: i-Bird RC Flyer http://www.silverlit-flyingclub.com/wingsmaster/

[2]ImageProc 2.4: https://github.com/biomimetics/imageproc_pcb

Variable	Test Parameters
Duty Cycle [Percent]	75,80,90,100
Angle of Attack [deg]	25,35,43,50,60
Wind Speed [m/s]	1.5,2.0,2.5
Elevator Deflection [deg]	-10,-6,0,8,19,30,35

TABLE I

TABLE OF TEST PARAMETERS USED FOR MEASUREMENTS COLLECTED IN THE WIND TUNNEL.

III. EXPERIMENTS AND RESULTS

A. Wind Tunnel

To determine the forces and moments that the ornithopter experiences in flight, wind tunnel data were collected over a series of trials using an ATI Nano17 force-torque sensor. The ornithopter was affixed to an acrylic mount attached to the sensor and facing into the air stream, as shown in Fig. 4. A 3 mm piece of foam was placed between the acrylic mount and the H^{2}Bird to provide damping for the high frequency oscillations that the flapping of the wings causes in the pitch moment signal. The H^{2}Bird was attached at approximately its center of mass, although this point fluctuates as the wings open and close. This fluctuation is minimal, however, so it was discounted in the data collection. For each trial, force and moment data were collected over a period of 7 seconds at all combinations of wing duty cycles, wind speeds, angles of attack, and elevator deflections shown in Table I, a total of 420 data sets. The wing motor duty cycle corresponds to flapping frequencies between 14 and 20 Hz, and a positive elevator deflection angle corresponds to an upward pitch. Each trial was averaged over the 7 seconds.

The collected data form a data set with 4 inputs and 3 outputs. The outputs are the lift force (L) and thrust force (T) in body coordinates, and the pitch moment (M), which are dependent upon the inputs of the duty cycle, angle of attack (α), wind speed (V), and elevator deflection, the directions of which are shown in the free body diagram in Fig. 5. In the diagram, the pitch angle, θ, is the angle between the horizontal in world coordinates and the x-axis, x_b, of the body of the H^{2}Bird, whereas the angle of attack, α, is the angle between the velocity vector and the x-axis of the body. This data set is used as a look-up table for the instantaneous

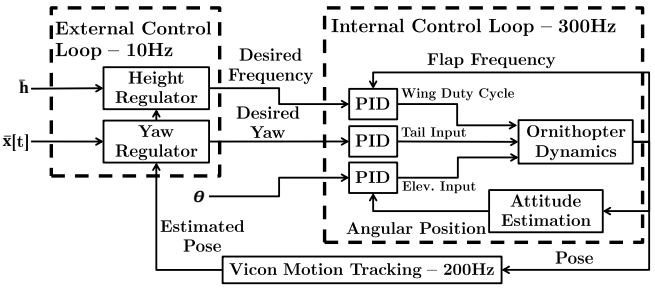

Fig. 3. Block diagram of the H^{2}Bird control system.

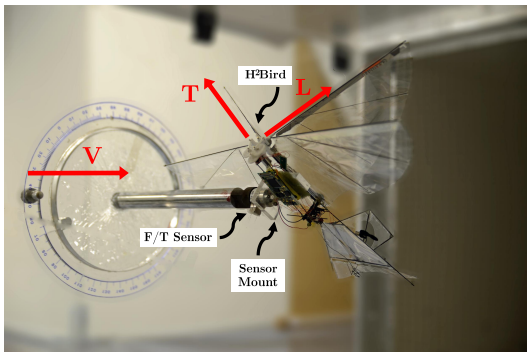

Fig. 4. Diagram of the H^{2}Bird mounted to the force-torque sensor in the wind tunnel [21].

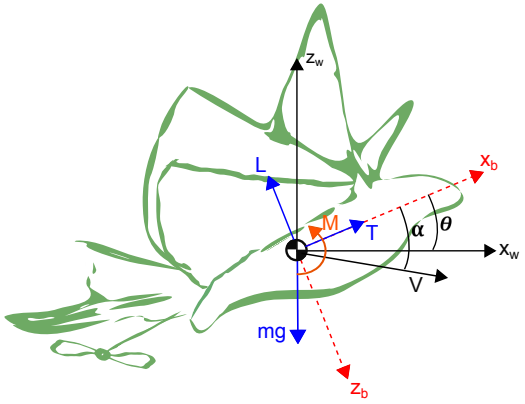

Fig. 5. Free body diagram of the H^{2}Bird for the wind tunnel experiment data.

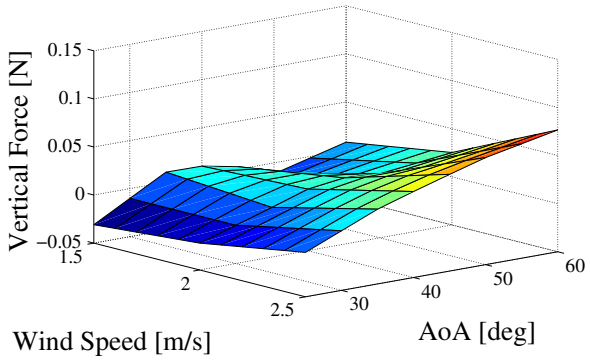

Fig. 6. A sample plot of the vertical force surface measured in the wind tunnel as a function of angle of attack and wind speed.

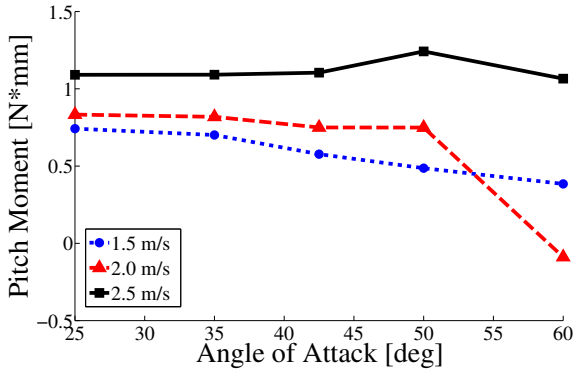

Fig. 7. The range of the change in pitch moment that the elevator can achieve for 80 percent duty cycle for different angles of attack and wind speeds. For example, at 40° angle of attack and 2.5 m/s wind speed, the elevator can affect a maximum change of about 1.1 N*m pitch moment through its entire range.

forces and moments for a given pose. The collected data form a series of surfaces similar to Fig. 6, which is the surface for a wing duty cycle of 80 percent and elevator deflection of 24 degrees. There are similar surfaces for each duty cycle and elevator deflection, and linear interpolation is used to estimate values between the measured data points. Fig. 7 shows a representation of the aerodynamic effect of the elevator as a function of angle of attack for increasing wind speeds. Each data point is the amplitude of the pitch moment provided by the elevator for a given operating point. As expected, the range of moments increases with increasing wind speed. The plot illustrates the control authority of the elevator available to influence the pitch of the ornithopter.

B. Free Flight

The free flight experiments were conducted over variable amounts of time during approximately straight and level flight of the H^{2}Bird. Before each experiment, the H^{2}Bird was launched by hand and directed to follow the path shown in Fig. 8 using the external control loop of Fig. 3. This desired path allows the completion of several experiments during a flight, and ensures that there is a straight and level portion of flight time in which to record a data set. A Vicon motion tracking system[3] was used to track the position of the H^{2}Bird at 200Hz, and this translational information was used with the desired reference trajectory, $x[t]$, shown in black in Fig. 8 as the input to a PID controller that computes the yaw angle necessary to maintain flight on the target path (black bar). A second PID controller was used to regulate the height of the H^{2}Bird at a constant height input, h, of 1.5 meters by computing the necessary flap frequency to maintain level flight. Throughout the reference path, the robot was directed to maintain a pitch angle of 35 degrees. The commanded angles and flap frequency were then transmitted to the robot at 10 Hz and the internal controllers on the H^{2}Bird moved the robot to the correct pose. When the H^{2}Bird reached the ends of the target path, it was directed to execute a 180 degree turn.

Each experiment consisted of a step from an initial pitch angle of 35 degrees to 50 degrees at 80 percent duty cycle. Each trial was conducted during the straight portion of the reference trajectory to minimize the effect of yaw and roll on the data. While straight and level flight was desired, some deviation occurred, although only trials with decidedly minimal disturbances were used in the data set. During the trials, the telemetry data, including the angular position, gyro values, and control motor inputs, were stored in the flash memory on the H^{2}Bird at 300 Hz. Additionally, the

[3]Vicon Motion Systems: http://www.vicon.com

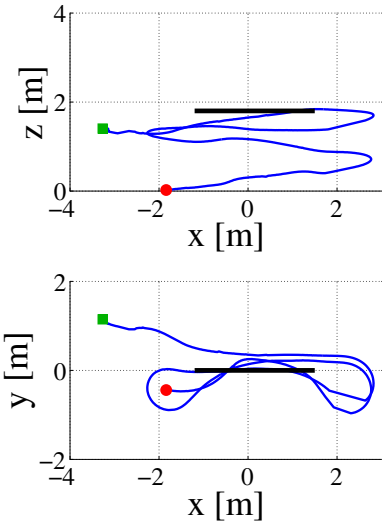

Fig. 8. Side and top views of a sample flight path with start point (green square) and stop point (red circle) in the tracking space. The black bar indicates the target path.

translational position and velocity, angular position, directed angles, and commanded flap frequency were stored from the Vicon at 200 Hz. The data for one trial are shown in Fig. 9, where the pitch angle, pitch velocity, and elevator deflection are estimated on the H^{2}Bird and the translational velocity is measured by the Vicon.

IV. COMPARISON OF DATA SETS

A. Equilibrium Point Estimation

We compare the free flight data set to the wind tunnel data set by determining the equilibrium flight points for both. The equilibrium points are flight conditions that satisfy the following criteria:

$$\begin{aligned} L_w &= mg \\ T_w &= D \\ \tau_P &= 0 \qquad (1) \\ \text{where} \qquad L_w &= T\sin\theta - L\cos\theta \\ T_w &= T\cos\theta + L\sin\theta \end{aligned}$$

where m is the mass of the H^{2}Bird, g is gravity, θ is the pitch angle, and τ_P is the total pitch moment. T is the thrust and L is the lift of the H^{2}Bird in body coordinates, shown in Fig. 5. D is the drag force, which balances the thrust in world coordinates, T_w. Since we can only know the forces and moments in free flight at equilibrium flight conditions, we can only directly compare these points to analogous points in the wind tunnel data.

To estimate the free flight equilibrium points, we computed the time averaged values for the velocity magnitude, pitch angle, angle of attack, and elevator deflection before and after the step from 35 to 50 degrees in pitch. The transitional portion during the step was not used in the analysis. We conducted 14 total trials, and the free flight equilibrium points are shown in the left half of Table II. Each of these

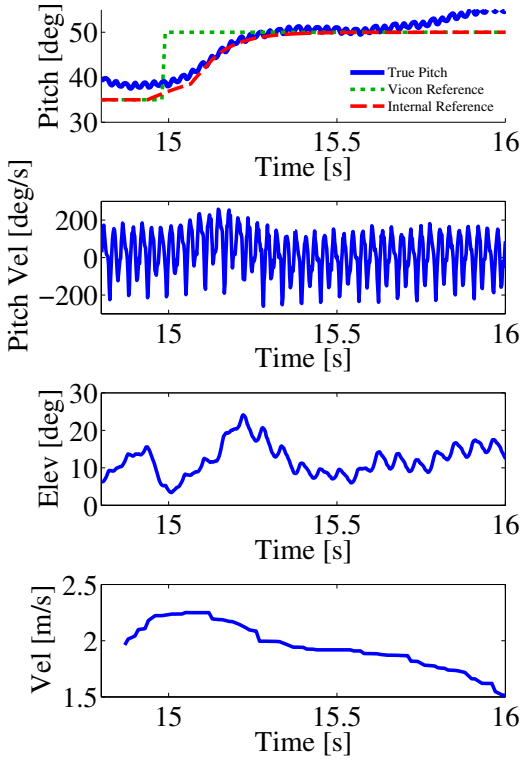

Fig. 9. The pitch, pitch velocity, elevator input, and velocity magnitude of the H^{2}Bird during one trial.

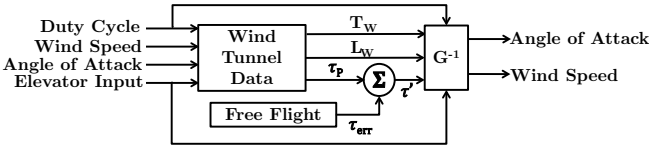

Fig. 10. Block diagram of the estimation of equilibrium points from the wind tunnel data.

equilibrium flight conditions was then used as the input into the wind tunnel lookup tables to determine the total horizontal and vertical forces in world coordinates and the total pitch moment predicted by the wind tunnel at these flight conditions. The results are in the right half of Table II, and correspond to the error between free flight and the wind tunnel data sets. Ideally, each each net force and moment should be zero at equilibrium.

Determining the predicted equilibrium points from the wind tunnel data is a more complicated process, outlined in Fig. 10. For a given duty cycle, wind speed, elevator input, and angle of attack there is an associated lift force, thrust force, and pitch moment measured in the wind tunnel. We used each elevator deflection and the 80 percent duty cycle used in the free flight experiments to generate three dimensional surfaces for the net thrust force, net lift force, and net pitch moment, each dependent upon the wind speed and angle of attack. Each of these surfaces are similar to the one in Fig. 6. For a given free flight trial, we computed the level sets at zero for each of the lift, thrust, and pitch moment surfaces for the particular elevator deflection in the

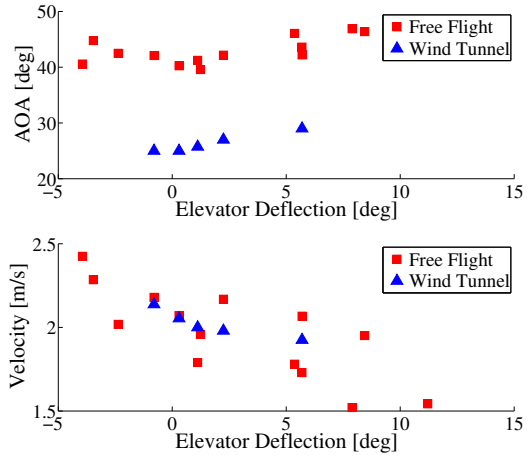

Fig. 11. Equilibrium points measured in free flight (red squares) and equilibrium points predicted from the wind tunnel (blue triangles).

trial. We noticed that, in most of the data, the pitch moment never crosses zero, and therefore, no equilibrium is predicted to exist in pitch. We attribute this problem to an error in the sensor placement, due to the approximation of the center of mass of the ornithopter. While this approximation has minimal effect on the lift and thrust force values, it will affect the magnitude of the pitch moment data. To remedy this problem, we added the mean optimal offset, $\tau_{err} = 0.77$ N*mm, uniformly over the entire data set to shift the wind tunnel predicted pitch moments for each equilibrium point in free flight as close as possible to zero. This optimal offset is the mean of the pitch moment errors in the eighth column of Table II, and the new values, τ', are in the ninth column. After this shift, we needed to find the equilibrium points in angle of attack and wind speed space predicted by the wind tunnel, which corresponds to the G^{-1} block in Fig. 10. To do this, we solved the optimization problem using the level sets at zero pitch moment:

$$\begin{aligned} \underset{\alpha,v}{\text{minimize}} \quad & F_T(\alpha,v)^2 + F_L(\alpha,v)^2 \\ \text{subject to} \quad & \tau' = 0 \end{aligned} \tag{2}$$

where α is angle of attack, v is velocity, F_L is the net vertical force, F_T is the net horizontal force, and τ' is the sum of the pitch moment from the wind tunnel data and the moment offset. The optimal α and v are recorded as the wind tunnel predicted equilibrium point for the given elevator deflection. These optimal values are the angle of attack and velocity on the zero pitch moment level set that minimizes the net vertical and horizontal forces. If any of the zero level sets do not exist for each of the three surfaces, we determine that there is no predicted equilibrium point for that particular operating condition.

B. Comparison of Estimations

The end result of the aforementioned process is a set of equilibrium points in velocity and angle of attack for which the wind tunnel predicts a zero pitch moment and minimal net vertical and horizontal force. The results of the estimation are in Fig. 11, where the blue triangles represent the wind tunnel predicted equilibrium points for the analogous free flight equilibrium points, represented by red squares, at a particular elevator deflection. There are five free flight points for which the wind tunnel predicts the existence of an equilibrium, and they lie between -2 and 6 degrees elevator deflection.

As shown in Fig. 11, the wind tunnel predicted equilibrium points in velocity are much closer to the free flight measurements with an average error of 0.1 m/s, than the predicted equilibrium points in angle of attack, which have an average error of 15 degrees. Numerically, the source of this error is evident in Table II in the "Net Thrust Force" and "Net Lift Force" columns. Both columns represent the total force in their respective directions and should be zero at equilibrium. The table shows that the wind tunnel underestimates the net thrust force for a given free flight data point, while it overestimates the net lift force for a given data point. With an H^{2}Bird weight of approximately 130 mN, the wind tunnel overestimates the net lift force by an average of 18 percent. Decreasing the angle of attack will decrease the drag and increase the lift caused by the airflow on the H^{2}Bird, moving both the net thrust force and net lift force closer to zero, hence the underestimation of the equilibrium in angle of attack by 15 degrees.

While the error in the wind tunnel predicted equilibrium points is easily explained numerically, the physical reasons for the error are more complex. Since the ornithopter is fixed in the wind tunnel, it is not free to pitch up and down as it does in free flight. The forces and moments caused by these changes in pitch velocity are not captured in the wind tunnel measurements. Additionally, there are high frequency vibrations, caused by the interaction between the frame of the robot and the mounting mechanism from the flapping of the wings, that introduce noise in the wind tunnel measurements, but are not present in free flight.

V. CONCLUSIONS

We have compared the predicted behavior of an ornithopter from a wind tunnel measured data set to measured free flight equilibrium conditions. As a comparison metric, we determined the equilibrium velocity magnitude and angle of attack predicted by the wind tunnel data set for given free flight measured elevator deflections. The wind tunnel equilibrium was represented as the angle of attack and velocity on the pitch moment level set at zero that minimizes the net horizontal and vertical forces measured in the wind tunnel. We found that the wind tunnel underestimates the angle of attack observed in free flight at equilibrium by approximately 15 degrees, whereas the error between the equilibrium velocities between the two data sets is approximately 0.1 m/s for an average flight speed of 2.0 m/s.

We intend to further examine the wind tunnel data to determine if, with some adjustments inspired by free flight measurements, it can be used to develop an aerodynamic model using a look-up table to predict the flight path of the

	Free Flight Measurements				Interpolated Net Wind Tunnel Values			
Trial Number	AOA deg	Velocity Mag m/s	Elevator Input deg	Pitch deg	Net Thrust Force mN	Net Lift Force mN	Pitch Moment N*mm	Adj. Moment N*mm
1	41	2.4	-4	46	-57	48	-0.56	0.21
2	40	2.0	-1	58	-63	10	-0.76	0.01
3	42	2.2	2	42	-25	38	-0.50	0.27
4	44	1.7	6	53	-41	13	-0.80	-0.03
5	42	2.1	6	38	-12	31	-0.47	0.30
6	46	1.8	5	52	-48	11	-0.93	-0.16
7	42	2.2	-1	42	-28	39	-0.59	0.18
8	47	1.5	11	50	-37	0	-1.12	-0.35
9	45	2.3	-3	45	-49	47	-0.86	-0.09
10	46	2.0	8	52	-55	17	-0.72	0.05
11	41	1.8	1	42	-11	21	-0.88	-0.11
12	40	2.1	0	41	-24.	29	-0.69	0.08
13	43	2.0	-2	44	-26	30	-0.76	0.01
14	47	1.5	8	53	-43	-2	-1.16	-0.39
			Mean		-37	24	-0.77	0.00
			Max Error		63	48	1.16	0.39
			Min Error		11	0	0.47	0.01

TABLE II

TABLE OF FREE FLIGHT MEASURED EQUILIBRIUM FLIGHT POINTS AND WIND TUNNEL PREDICTED THRUST AND LIFT FORCES AND PITCH MOMENT. IDEALLY, THE NET THRUST FORCE, NET LIFT FORCE, AND PITCH MOMENT SHOULD ALL BE ZERO AT THE FREE-FLIGHT MEASURED EQUILIBRIUM POINTS.

robot. A simpler data-based model will enable us to control the robot more accurately without great computational overhead.

ACKNOWLEDGMENT

The authors thank Fernando Garcia Bermudez for his assistance with data collection from the Vicon motion capture system and the members of the Biomimetic Millisystems Laboratory and the EECS community at the University of California, Berkeley for their advice and support.

REFERENCES

[1] H. Liu and K. Kawachi, "Leading-edge vortices of flapping and rotary wings at low Reynolds number." *Progress in Astronautics and Aeronautics*, vol. 195, pp. 275–285, 2001.

[2] R. Ames, O. Wong, and N. Komerath, "On the flowfield and forces generated by a flapping rectangular wing at low Reynolds number." *Progress in Astronautics and Aeronautics*, vol. 195, pp. 287–305, 2001.

[3] D. Lentink, G. F. van Heijst, F. T. Muijres, and J. L. van Leeuwen, "Vortex interactions with flapping wings and fins can be unpredictable," *Biology Letters*, vol. 6, pp. 394–397, 2010.

[4] G. C. H. E. de Croon, K. M. E. de Clercq, R. Ruijsink, B. Remes, and C. de Wagter, "Design, aerodynamics, and vision-based control of the DelFly," *International Journal of Micro Air Vehicles*, vol. Vol. 1, no. 2, pp. 71–97, June 2009.

[5] B. Cheng and X. Deng, "Translational and rotational damping of flapping flight and its dynamics and stability at hovering," *IEEE Transactions on Robotics*, vol. Vol. 27, no. 5, pp. 849–864, 2011.

[6] J. Han, J. Lee, and D. Kim, "Ornithopter modeling for flight simulation," in *Intl. Conf. on Control, Automation and Systems*, 2008, pp. 1773–1777.

[7] A. T. Pfeiffer, J. Lee, J. Han, and H. Baier, "Ornithopter flight simulation based on flexible multi-body dynamics," *Journal of Bionic Engineering*, vol. Vol. 7, no. 1, pp. 102 – 111, 2010.

[8] M. A. Bolender, "Rigid multi-body equations-of-motion for flapping wing mavs using kanes equations," in *AIAA Guidance, Navigation, and Control Conference*, 2009.

[9] J. Grauer and J. Hubbard, "Multibody model of an ornithopter," in *Journal of Guidance, Control, and Dynamics*, vol. 32, no. 5, Sept. - Oct. 2009, pp. 1675–1679.

[10] C. Orlowski and A. Girard, "Modeling and simulation of nonlinear dynamics of flapping wing micro air vehicles," *AIAA Journal*, vol. 49, no. 5, pp. 969–981, May 2011.

[11] S. Baek, F. G. Bermudez, and R. Fearing, "Flight control for target seeking by 13 gram ornithopter." in *IEEE Intl. Conf. on Intelligent Robots and Systems*, 2011, pp. 2674–2681.

[12] S. Baek and R. Fearing, "Flight forces and altitude regulation of 12 gram i-bird," in *IEEE Intl. Conf. on Biomedical Robotics and Biomechatronics*, 2010, pp. 454–460.

[13] Z. Khan and S. Agrawal, "Control of longitudinal flight dynamics of a flapping-wing micro air vehicle using time-averaged model and differential flatness based controller," in *American Control Conference*, 2007, pp. 5284–5289.

[14] L. Schenato, D. Campolo, and S. Sastry, "Controllability issues in flapping flight for biomimetic micro aerial vehicles (MAVs)," in *42nd IEEE Conf. on Decision and Control*, vol. 6, 2003, pp. 6441–6447.

[15] W. B. Dickson, A. D. Straw, C. Poelma, and M. H. Dickinson, "An integrative model of insect flight control," in *44th American Institute of Aeronautics and Astronautics Sciences Meeting*, 2006.

[16] S. Sane and M. Dickinson, "The aerodynamic effects of wing rotation and a revised quasi-steady model of flapping flight," *Journal of Experimental Biology*, vol. Vol. 205, no. 8, pp. 1087–1096, 2002.

[17] Z. A. Khan and S. K. Agrawal, "Force and moment characterization of flapping wings for micro air vehicle application," in *American Control Conference*, 2005.

[18] D.-K. Lee and J.-H. Han, "Flight controller design of a flapping-wing MAV in a magnetically levitated environmentl," in *Intl. Conf. on Robotics and Automation*, 2013.

[19] R. Julian, C. Rose, H. Hu, and R. Fearing, "Cooperative control for window traversal with an ornithopter MAV and lightweight ground station," in *12th Intl. Conf. on Autonomous Agents and Multiagent Systems, 2013. Proceedings*, 2013.

[20] J. Grauer, E. Ulrich, J. Hubbard Jr., D. Pines, and J. Humbert, "System identification of an ornithopter aerodynamics model," in *AIAA Atmospheric Flight Mechanics Conference*, Aug. 2010.

[21] C. Rose and R. S. Fearing, "Flight simulation of an ornithopter," Master's thesis, EECS Department, University of California, Berkeley, May 2013. [Online]. Available: http://www.eecs.berkeley.edu/Pubs/TechRpts/2013/EECS-2013-60.html